

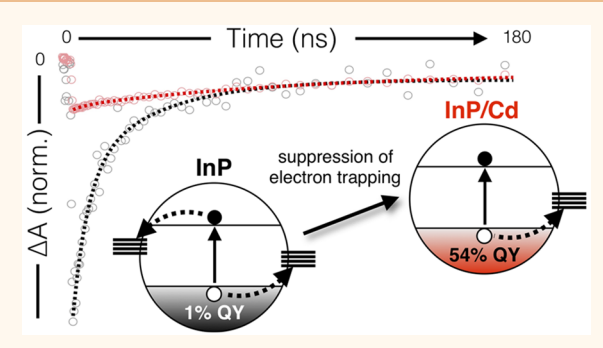
Effects of Surface Chemistry on the Photophysics of Colloidal InP Nanocrystals

Kira E. Hughes, Jennifer L. Stein, Max R. Friedfeld, Brandi M. Cossairt, * and Daniel R. Gamelin *

Department of Chemistry, University of Washington, Seattle, Washington 98195-1700, United States

Supporting Information

ABSTRACT: Indium phosphide (InP) semiconductor nanocrystals (NCs) provide a promising alternative to traditional heavymetal-based luminescent materials for lighting and display technologies, and implementation of InP NCs in consumer products is rapidly increasing. As-synthesized InP NCs typically have very low photoluminescence quantum yields (PLQY), however. Although empirical methods have led to NCs with near-unity PLQYs, a fundamental understanding of how specific synthetic and post-synthetic protocols can alter the electronic landscape of InP NCs is still lacking. Here, we have studied a series of homologous InP NCs prepared from InP clusters using a combination of room-temperature and low-temperature time-



resolved spectroscopies to elucidate how specific charge-carrier trapping processes are affected when various surface modifications are performed. The data allow identification of large PLQY increases that occur specifically through elimination of surface electron traps and provide a rationale for understanding the microscopic origins of this trap suppression in terms of elimination of undercoordinated surface In³⁺ ions. Despite essentially complete elimination of surface electron trapping when surface In³⁺ is addressed, hole trapping still exists. This hole trapping is shown to be partially suppressed by even very thin shell growth, attributable to elimination of undercoordinated surface phosphides. We also observe signatures of bright-dark excitonic splitting in InP NCs with only submonolayer surface coverage of select additives (divalent Lewis acids or fluoride anions)-signatures that have only been previously observed in thickshelled InP NCs. Together, these synthetic and spectroscopic results improve our understanding of relationships between specific InP NC surface chemistries and the resulting NC photophysics.

KEYWORDS: nanocrystals, indium phosphide, photoluminescence, carrier trapping, quantum yield

olloidal semiconductor nanocrystals (NCs) are the subject of intense research for application in a variety of technologies including solar energy conversion, biological imaging, and solid-state lighting. Colloidal semiconductor NCs display tunability of their absorption and photoluminescence (PL) energies and can emit with narrow PL linewidths, making them attractive as downconversion phosphors for wide-color-gamut displays.² As incorporation of these materials into consumer products increases, however, concerns over heavy-metal-based NCs have refocused research toward less toxic materials. Indium phosphide (InP) NCs are a proven alternative to traditional cadmium- and lead-based chalcogenide NCs. InP NCs are less toxic than traditional cadmium selenide (CdSe) NCs, 3,4 reducing environmental and health concerns. Their larger Bohr radius compared to CdSe also allows absorption and PL energies to be tuned across a wider spectral window,5 which is of interest for display technologies. Despite these advantages, chemical issues still persist that must be addressed before InP NCs become the material of choice for widespread industrial phosphor applications. In particular, as-synthesized InP NCs generally

exhibit low (~1%) photoluminescence quantum yields (PLQYs), relatively broad ensemble PL linewidths, and substantial midgap luminescence because of numerous surface defects that introduce deep charge-carrier trap states. Furthermore, even with substantial modification of InP NC cores, they cover the desired color gamut less effectively and with lower internal quantum efficiencies than more-toxic CdSe

To improve the performance of colloidal InP NCs, it is necessary to develop synthetic procedures that can control their photophysics and suppress undesired carrier trapping. Unfortunately, little is known about the microscopic identities of carrier traps in InP NCs. $^{7-10}$ There is even little consensus about the relative importance of electron vs hole trapping in determining the PLQYs of InP NCs. For example, low PLQYs have been attributed not only to electron trapping at undercoordinated indium sites (aka, phosphorus vacancies)^{7,9} but

Received: September 4, 2019 Accepted: November 15, 2019 Published: November 15, 2019



also to hole trapping at under-coordinated phosphorus sites. 6,11 High PLQYs have mainly been obtained by growing thick or gradient shells onto InP NC surfaces. 12-14 For example, a 95% PLQY was recently reported for InP/ZnSe/ZnS NCs.¹³ Some reports have described increased InP NC PLQYs after etching with HF to remove surface traps. 15-18 From ultrafast spectroscopic studies of as-synthesized, HFtreated, and ZnS-shelled InP NCs, one study noted a lack of correlation between PLQY and transient absorption (TA) bleach recovery, pointing to an absence of electron trapping. The presence of a rapid PL decay component (on a ~600 ps window) that was absent from the TA dynamics indicated rapid hole trapping, and growth of a ZnS shell was shown to reduce this hole trapping. 10 On the other hand, electron trapping at under-coordinated indium sites was concluded from optically detected magnetic resonance (ODMR) data, which showed a resonance broadened by hyperfine interactions with indium nuclei.9 A deeper fundamental understanding of the influence of surface chemistry on the PL of colloidal InP NCs will help to improve the quality and reliability of these materials for next-generation display and spectral-conversion technologies.

Here, we describe spectroscopic studies of a series of five homologous InP NC samples that collectively allow systematic investigation into the effects of different surface chemistries on charge-carrier trapping, and hence on InP NC PLQYs. Assynthesized InP NCs made from InP clusters have indium-rich surfaces 19 and show low (\sim 1%) PLQYs, consistent with undercoordinated surface indium ions acting as electron traps. Postsynthetic reaction of these InP NCs with metal-carboxylates induces surface cation exchange¹⁹ and vastly increases the PLQY (up to ~50%). Synthesizing the InP NCs in the presence of fluorinated ionic liquids forms surface In-F bonds¹⁷ and yields NCs with PLQYs up to \sim 20%, successfully replicating the results of HF etching.²⁰ Shell growth also increases the PLQY.^{12–14,21} Variable-temperature (VT) PL and TA measurements reveal that the PLQY increases observed across this series of NC samples stem primarily from elimination of surface electron traps and show that electron trapping can be effectively completely eliminated with these chemistries. Even with essentially complete suppression of electron trapping, however, the PLQYs reach only ~50%, and hole trapping is still observed. These results demonstrate that the PLQYs of the as-synthesized InP NCs depend quite substantially on both electron and hole trapping. Notably, VTPL measurements of InP NCs with submonolayer surface modifications reveal clear signatures of exciton fine-structure splittings that in the past have only been observed after growth of thick high-quality shells, highlighting the efficacy of the targeted surface modifications described here for reducing nonradiative carrier recombination losses in colloidal InP NCs. These findings advance our understanding of surface traps in colloidal InP NCs and contribute to the development of welldefined chemical tools for suppressing carrier trapping in these technologically important materials.

RESULTS AND DISCUSSION

Sample Preparation and General Characterization. Figure 1 presents transmission electron microscope (TEM) images of InP NCs ($d=2.7\pm0.4$ nm), InP/F NCs ($d=2.4\pm0.3$ nm), InP/Zn NCs ($d=2.7\pm0.3$ nm), and InP/Cd NCs ($d=2.7\pm0.3$ nm), all synthesized from carboxylate-ligated InP clusters. All of these NCs have quasi-spherical shapes and

similar sizes except the InP/F NCs, whose average NC diameter is slightly smaller than those of the others $(2.4 \text{ } \nu \text{s} \text{ } 2.7 \text{ } \text{nm})$.

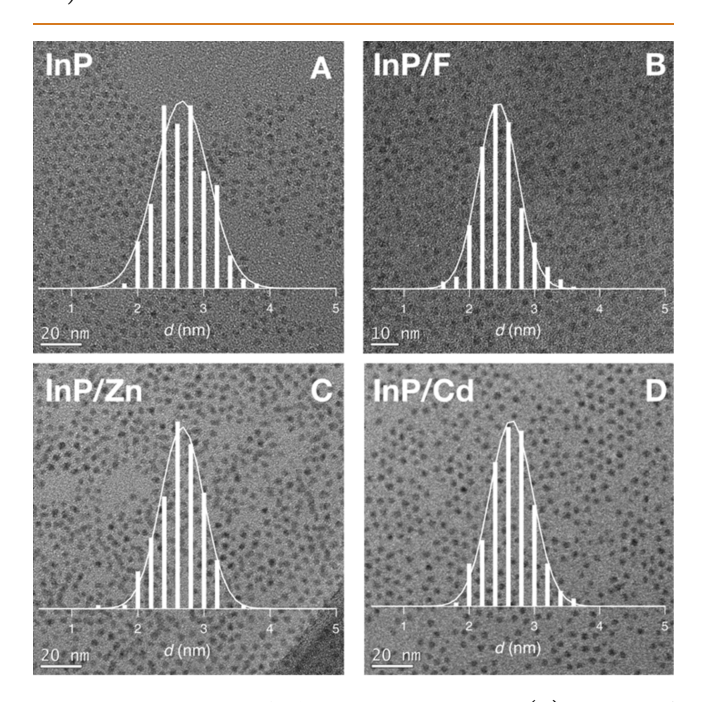


Figure 1. TEM images of selected InP NC samples. (A) InP NCs, $d=2.7\pm0.4$ nm, (B) InP/F NCs, $d=2.4\pm0.3$ nm, (C) InP/Zn NCs, $d=2.7\pm0.3$ nm, and (D) InP/Cd NCs, $d=2.7\pm0.3$ nm.

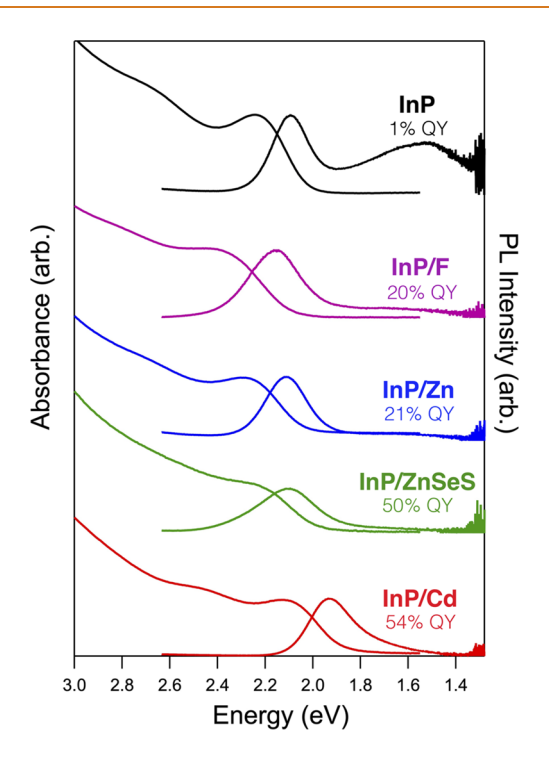


Figure 2. Absorption (left) and CW PL (right) of the InP NCs (black, 1% PLQY), InP/F NCs (fuchsia, 20% PLQY), InP/Zn NCs (blue, 21% PLQY), InP/ZnSeS NCs (green, 50% PLQY, ~1.2 nm shell thickness, ~9:1 Se:S), and InP/Cd NCs (red, 54% PLQY) that were used in this study. All samples were made from InP clusters. All data were collected on colloids in toluene at room temperature. The NC diameter stays roughly the same despite shifts of the first excitonic transition across the sample series.

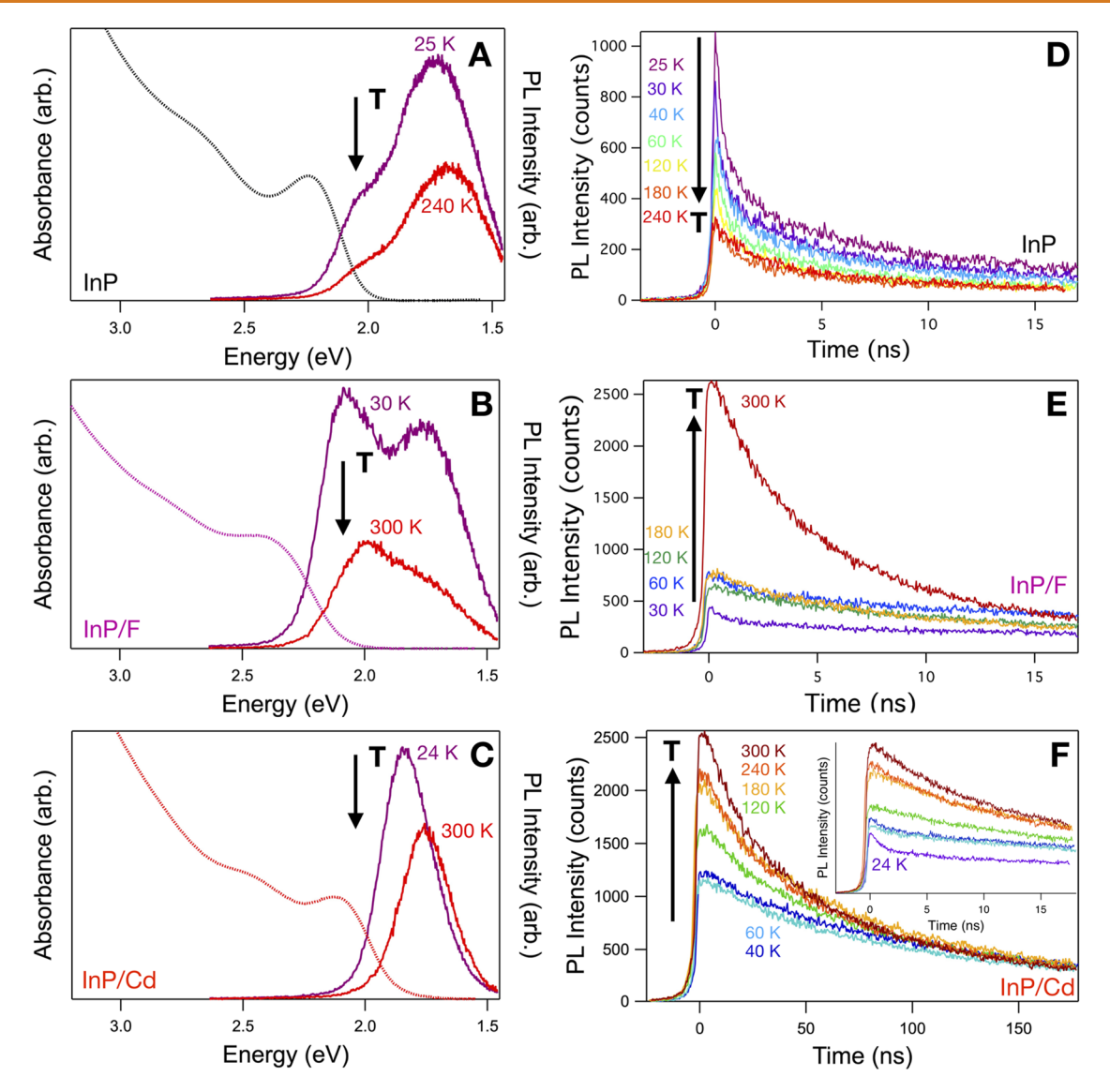


Figure 3. (A–C) Room-temperature absorption spectra (dotted), VT PL spectra (solid), and (D–F) VT excitonic PL decay dynamics measured for various InP NCs. Data were collected at temperatures between 24 and 300 K for (A, D) as-prepared InP NCs, (B, E) InP/F NCs, and (C, F) InP/Cd NCs. PL spectra were obtained by integrating streak-camera data over 1 μ s. PL decay curves were obtained by integrating between ~2.15 and 2.00 eV for the InP NCs, between ~2.20 and 2.00 eV for the InP/F NCs, and between ~1.95 and 1.75 eV for the InP/Cd NCs. Note the much longer time window in panel F. For comparison, the inset plots the same data on the same time window as in panels D and E.

Figure 2 summarizes the absorption and continuous wave (CW) PL of the same series of NC samples shown in Figure 1, plus an additional InP/ZnSeS core/shell NC sample (~1.2 nm shell thickness, ~9:1 Se:S). The spectra are presented in order of increasing PLQY. The untreated InP NCs show a first excitonic absorption maximum at 2.24 eV and exhibit a low (<1%) excitonic PLQY accompanied by broad trap emission to lower energy. Synthesis of the NCs in the presence of fluorinated ionic liquids (InP/F, see Methods) increases the PLQY to 20%. The first excitonic absorption maximum is blueshifted by ~180 meV to ~2.24 eV, and the trap PL is reduced relative to the excitonic PL. Annealing the as-prepared InP NCs in the presence of Zn-carboxylates forms InP/Zn NCs, which show a slight blue-shift of 60 meV, moving the first excitonic absorption maximum to ~2.3 eV. These NCs show an excitonic PLQY of 21%, and the low-energy trap PL is nearly indistinguishable from the baseline. Growth of a thin ZnSeS shell (\sim 1.2 nm, \sim 9:1 Se:S) on the as-prepared InP NCs

broadens the first excitonic absorption (centered at ~2.25 eV) and PL bands and increases the PLQY to 50%. Lastly, InP/Cd NCs synthesized by annealing InP NCs in the presence of Cd-carboxylate show a first excitonic absorption maximum that is red-shifted from that of the as-prepared InP NCs by ~120 meV (to 2.12 eV), and they have a PLQY of 54%. The PL band appears to have an asymmetric shape, tailing to lower energies. These results demonstrate that InP NC surface modifications can dramatically increase PLQYs (from <1% to 54%) and shift band-edge absorption by nearly 200 meV without significantly changing the NC size.

Variable-Temperature Photoluminescence. Figure 3 summarizes VTPL data collected for InP, InP/F, and InP/Cd NCs. Figure 3A—C shows VTPL spectra of these NC samples in comparison with their room-temperature absorption spectra. The PLQY and the ratio of excitonic to trap PL intensities both increase across this series of samples. For all three samples, the excitonic PL shifts to lower energy and decreases

in intensity with increasing temperature, as reported previously. 8,22–24 The PL intensities of all three samples also decrease with increasing temperature. Figure 3D–F shows excitonic PL decay dynamics measured as a function of temperature for the same series of NCs. All three samples show multiexponential (quasi-biexponential) decay at all temperatures, and the PL decay half-life increases in conjunction with the increasing PLQY. For each sample, the PL decay curves appear to converge to a similar slow decay time at all temperatures. At short times (0–3 ns), however, the InP/F and InP/Cd NCs (Figure 3E,F) both show decay components whose amplitudes *increase* with increasing temperature. This temperature dependence contrasts that of the InP NCs (Figure 3D), whose excitonic PL intensity merely decreases with increasing temperature on all time scales.

To explore the anomalous temperature dependence observed in Figure 3, Figure 4A plots the integrated short-

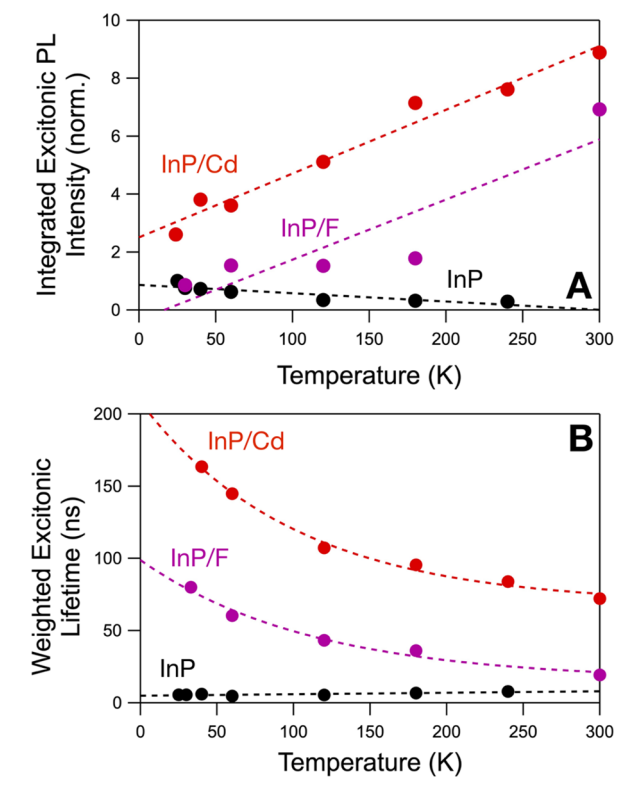


Figure 4. (A) Excitonic PL intensities integrated over short times (0-3 ns), plotted as a function of temperature for the InP NCs (black), InP/F NCs (fuchsia), and InP/Cd NCs (red) described by Figure 3. (B) Weighted-average excitonic PL decay times plotted as a function of temperature for the same three NC samples. The excitonic PL decay of the InP NCs slows slightly with increasing temperature, but the excitonic PL decay of the InP/F and InP/Cd NCs accelerates with increasing temperature. The dashed lines are guides to the eye.

time (0–3 ns) excitonic PL intensities of each sample *vs* temperature. Whereas the InP PL intensity decreases with increasing temperature, the short-time excitonic PL intensities of the InP/Cd and InP/F NCs both continue to increase with increasing temperature, all the way up to room temperature. This trend in spectral intensities is unusual and to our knowledge has not been noted previously for other unshelled InP NCs. An increase in time-integrated excitonic PL intensity with increasing temperature has been reported for InP/ZnS

core/shell NCs. ²⁵ Figure 4B plots the weighted-average excitonic PL decay times for these three samples as a function of temperature (see SI for fitting). For the InP NCs, the average PL decay time increases slightly from \sim 5.5 ns at 25 K to \sim 8.0 ns at 240 K, but for the InP/F NCs the average PL decay time *decreases* from 80 ns at 33 K to \sim 20 ns at 300 K, and for the InP/Cd NCs it also decreases, from \sim 165 ns at 40 K to \sim 70 ns at 300 K. The decreasing PL decay times in Figure 4B combined with the increasing short-time PL intensities in Figure 4A indicate that radiative recombination at short times accelerates with increasing temperature in these NCs. In the as-prepared InP NCs, this behavior is obscured by rapid nonradiative decay (PLQY < 1%), but this trend in radiative decay rates becomes evident in the InP/Cd and InP/F NCs where the PLQYs are greater.

Electron vs Hole Trapping. Figure 5 presents room-temperature TA bleach-recovery dynamics measured at the bleach maximum (see inset for TA spectra) and normalized at t = 0 for each of the NCs in the series described above. For comparison, Figure 5 also plots excitonic and midgap trap-state

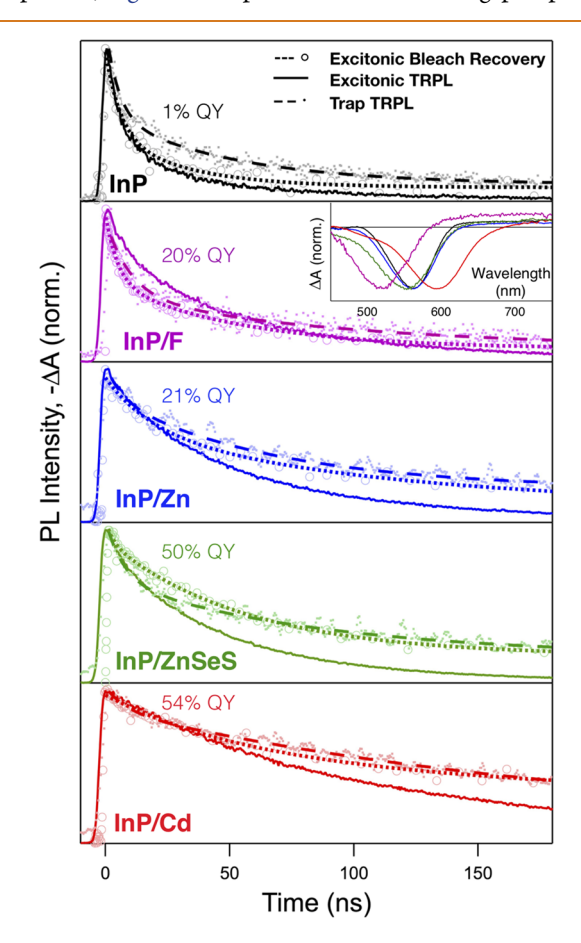
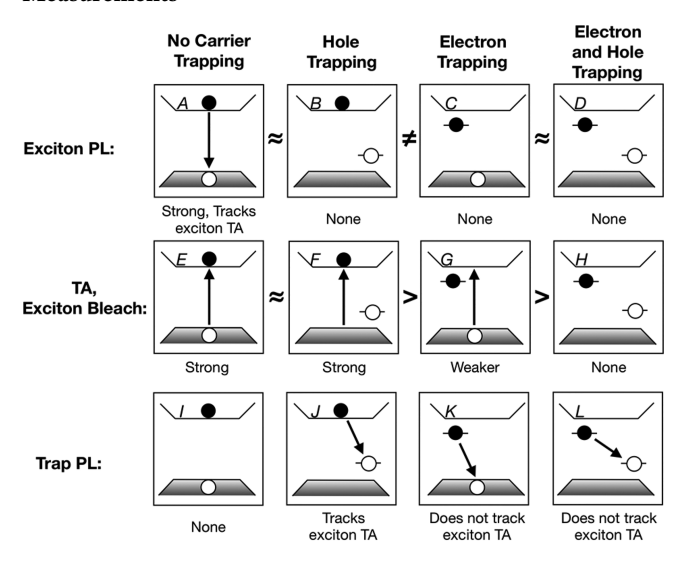


Figure 5. Normalized room-temperature excitonic TA bleach recovery (circles and short-dashed lines, inverted for comparison with other data), excitonic TRPL decay (solid lines), and trap TRPL decay (dots and long-dashed lines) data for all five InP NC samples examined here, presented in order of increasing PLQY. All data were collected at room temperature on NCs suspended in toluene. The untreated InP NCs (black) show the fastest decay in all three measurements as well as the lowest PLQY. The excitonic TRPL decays most quickly, with the greatest difference at long times seen for NCs with the highest PLQYs. Inset: Normalized TA spectra for all five samples, following the same color scheme.

PL decay dynamics for each sample (see Figure 3). The TA bleach-recovery curves have been inverted for comparison with the other dynamics data. The samples are presented in order of increasing PLQY to illustrate a general trend of slower dynamics within the first ~ 50 ns associated with higher PLQYs. Normalization at t=0 also highlights a rough trend of increasing divergence between TA and excitonic time-resolved photoluminescence (TRPL) decay curves at long times with increasing PLQY.

To interpret the trends in Figure 5, we take advantage of the different sensitivities of the TA and PL measurements to different types of charge carriers, as established previously ^{26–29} and summarized in Scheme 1; whereas excitonic TRPL reports

Scheme 1. Illustration of Charge-Carrier Processes Probed by Band-Edge TA, Excitonic TRPL, and Trap-State TRPL Measurements a



"Note that panels J and K are only approximate because the difference in TA sensitivity for electrons and holes is roughly a factor two.

on the dynamics of conduction-band (CB) electron and valence-band (VB) hole pairs (Scheme 1A), band-edge TA bleach-recovery dynamics are dominated by contributions from the CB electron population (Scheme 1E,F), with the VB hole contributing less to the bleach amplitude because of the greater VB degeneracy. Trap-state PL dynamics can reflect primarily either the CB electron or VB hole dynamics depending on the specific configuration of the luminescent excited state (Scheme 1J or K), or they can reflect neither in the scenario where both carriers are localized (Scheme 1L). Given these considerations, it is possible to deduce information about the photogenerated excited states from the comparison of TA and TRPL dynamics.

For the as-prepared InP NCs, the TA and excitonic TRPL signals in Figure 5 both decay with the same dominant time constant of $\tau \sim 7$ ns, and the trap-state PL follows much the same dynamics. From Scheme 1, we interpret this $\tau \sim 7$ ns process as trapping of CB electrons. The observation that the trap-state PL decays with the same $\tau \sim 7$ ns time constant supports assignment of this trap-state PL as involving recombination of a CB electron with a deeply trapped hole, and it further indicates that some extent of hole trapping occurs on time scales faster than our measurement window. This latter conclusion is consistent with previous reports of

subnanosecond hole trapping in InP NCs. ¹⁰ The exciton PL decays to nearly zero with this $\tau \sim 7$ ns time constant, consistent with the low excitonic PLQY of these NCs being in part attributable to electron trapping, but the TA bleach and the trap-state PL both show significant amplitudes (rel.) at long times, which also suggests a population of CB electrons that decays slowly via radiative recombination with deeply trapped holes (*i.e.*, by trap-state PL).

Moving down the NC series toward higher excitonic PLQYs, the key trends are (i) elimination of the $\tau \sim 7$ ns component in the exciton TA bleach and PL dynamics and (ii) more prominent differences between excitonic PL and TA (or trapstate PL) amplitudes at long times. In the InP/Cd NCs, which have the highest excitonic PLQYs, the $\tau \sim 7$ ns decay component is almost completely absent, suggesting almost complete elimination of CB electron trapping. This trend suggests a correlation between the $\tau \sim 7$ ns process and the NC PLQY and, hence, supports the conclusion that InP NC PLQYs are at least in part determined by CB electron-trapping dynamics.

To underscore this result, the TA bleach-recovery curves from Figure 5 are replotted in Figure 6A normalized at long

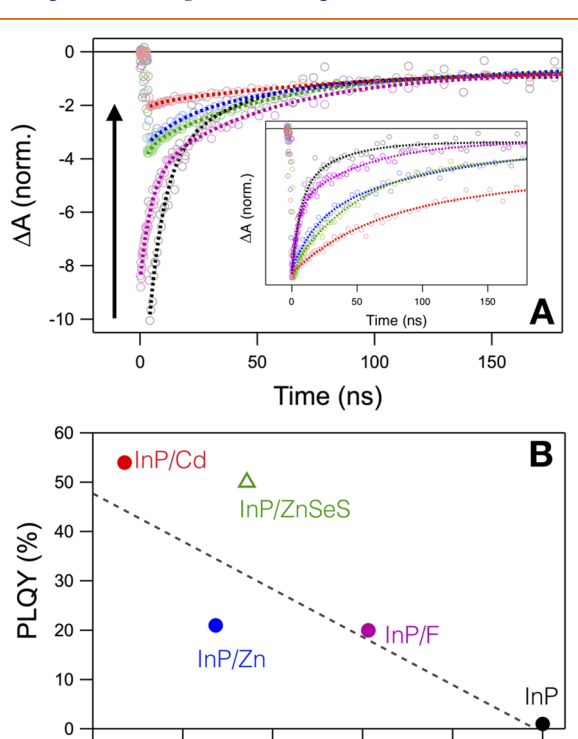


Figure 6. (A) Room-temperature TA exciton bleach-recovery dynamics normalized at t=120 ns for all of the InP NC samples from Figure 5. The InP NCs (1% PLQY) show the most (rel.) bleach recovery at early times, and the InP/Cd NCs (54% PLQY) show the least. Inset: The same curves normalized at t=0 ns. (B) Exciton PLQYs for InP, InP/F, InP/Zn, InP/Cd NCs (circles), and InP/ZnSeS NCs (open triangle), plotted as a function of the normalized integrated fast TA bleach recovery. The x-axis values were obtained by fitting the TA bleach-recovery dynamics normalized at 120 ns to a biexponential function on a 200 ns time window and integrating the fast-decay component. The dashed line shows a best-fit line to the circular data points.

0.4

0.6

Integrated Intensity of Fast

TA Decay Component (norm.)

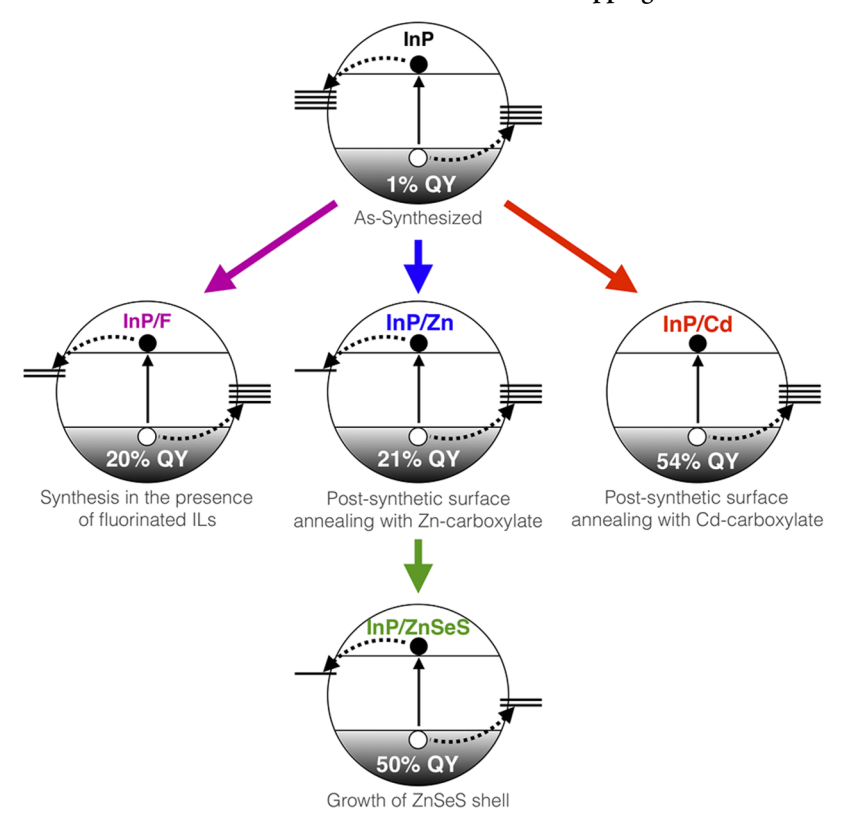
0.8

0.2

0.0

1.0

Scheme 2. Effects of Different Surface Chemistries on Electron and Hole Trapping in InP NCs



times (t > 120 ns). (The inset shows the same data normalized at t = 0.) This representation of the data reveals a clear correlation between the TA amplitude at short times and the PLQY. To quantify this relationship, Figure 6B plots excitonic PLQY vs the normalized integrated intensity of the fast TA component for each sample, obtained by fitting each TA trace to a biexponential function and then integrating just the fast component (see SI for numerical results). Figure 6B reveals an inverse correlation between PLQY and the amount of fast TA bleach recovery. A qualitatively similar conclusion is reached without any fitting, by just plotting the y intercept of the data in Figure 6B vs PLQY (see SI). This correlation provides strong evidence that the surface modifications performed here help to increase NC PLQYs by suppressing CB electron trapping on the \sim 7 ns time scale. Interestingly, the best-fit line describing the InP, InP/F, InP/Zn, and InP/Cd NCs does not intercept the y axis at PLQY = 100%, but instead it intercepts at PLQY \sim 50% (\pm 4%). This observation suggests that elimination of electron traps alone in this series of NC samples can only increase their PLQYs to \sim 50%. The remaining \sim 50% nonradiative decay is presumably attributable to hole trapping. The absence of any significant \sim 7 ns decay component for the InP/Cd NCs and the 54% PLQY for these NCs thus suggest that it is possible to eliminate electron trapping almost entirely by simple surface modification with Cd²⁺, but to achieve unity PLQY, the remaining hole trapping must also be eliminated. The Cd²⁺, Zn²⁺, and F⁻ surface modifications described here appear to have little influence on such hole trapping. All three modifications described here specifically affect surface cations but not surface anions (i.e., P³⁻), either by reducing the number of surface In³⁺ (through cation exchange) or by formation of surface In-F bonds. Among the samples investigated here, only the InP/ZnSeS NCs also involve

modification of the surface anions, burying surface phosphides to leave only sulfide and selenide anions at the NC surfaces. As such, it is tempting to interpret the comparison between InP/Zn and InP/ZnSeS NCs as attributable to additional suppression of hole trapping; both samples show similar PL losses to electron trapping, as gauged by their similar integrated fast TA decay, but the PLQY of the InP/ZnSeS NCs is more than double that of the InP/Zn NCs.

Discussion of the Results. For nearly two decades, intense research has been dedicated to the development of bright InP NCs with narrow PL linewidths and high PLQYs, ^{12,13,17,19,20,31–33} largely motivated by the prospect of using such low-toxicity materials as spectral-conversion phosphors in next-generation lighting and display technologies. Like for many semiconductor NCs, the surfaces of InP NCs are the source of many nonradiative recombination losses. In most cases, however, it has not been easy to connect synthetic improvements in NC PLQY with specific surface moieties or trapping processes, and consequently the major source(s) of nonradiative recombination remain poorly understood. Timeresolved spectroscopic evidence has pointed specifically to hole trapping as the primary limitation to high PLQYs in InP NCs, 10 but ODMR data have suggested predominant electron trapping in InP NCs, reflecting uncertainty in the relative abundance and microscopic identities of various InP NC surface traps.

In the present study, we have sought to understand the effects of specific surface chemistries on carrier trapping in colloidal InP NCs. Using a series of closely related samples all prepared from InP clusters, we have demonstrated substantial increases in PLQY when the NC surfaces are modified not only by growth of ZnSeS shells but also by simple binding of Cd²⁺, Zn²⁺, and F⁻ ions. With this series of related NCs in

hand, TA and TRPL spectroscopies were then used to investigate which carrier-recombination processes are affected by these surface modifications. The data from these experiments suggest that both electron and hole trapping contribute substantially to nonradiative decay in the parent InP NCs prior to surface modification. The data further show that electron trapping can be selectively suppressed and almost completely eliminated by simple surface modifications involving addition of submonolayer surface Zn²⁺, F⁻, or particularly Cd²⁺. Elimination of electron trapping increases the NC PLQYs only up to ~50%, however, indicating that hole and electron trapping are approximately equally substantial in the initial asprepared InP NCs. ZnSeS shell growth appears to partially eliminate hole trapping as described previously, 10 but it does not eliminate electron-trapping sites as effectively as Cd2+ modification alone.

These trends are explained by the observation that all of the sample modifications examined here directly affect the NC surface cations; Cd²⁺ and Zn²⁺ replace surface-terminating In³⁺, and F⁻ modification leads to strong In–F bonds at the NC surfaces. Notably, our group has previously confirmed the absence of additional surface oxidation upon treatment with cadmium and zinc carboxylates. ^{19,34} Instead, displacement of indium carboxylate by Cd²⁺ or Zn²⁺ leads to independent nucleation of indium oxide in the form of \sim 10 nm particles as evidenced by TEM and X-ray diffraction analysis. f9 Detailed characterization of the NC surfaces following treatment with Cd²⁺, Zn²⁺, and F⁻ are provided in the literature. ^{17,19,34,35} All three modifications suppress electron trapping, consistent with such trapping involving surface In³⁺ cations. Shelling the NCs with ZnSeS appears to have all of the advantages of replacing surface In3+ with Zn2+, and additionally partially suppresses hole trapping. The observation that Se/S anion termination of InP NC surfaces reduces hole trapping is consistent with such trapping involving surface phosphide moieties. These trends across the entire series of NC samples investigated here are summarized in Scheme 2.

An interesting observation is that InP NC surfaces terminated by F are less prone to electron trapping than those terminated by O₂CR. This observation suggests specifically that undercoordinated In³⁺ serves as an electrontrapping site; F⁻ binds In³⁺ more strongly than carboxylates do while being sterically small and occupying only a single coordination site, reducing the probability of undercoordinated surface In³⁺. This conclusion is consistent with the observation that addition of Cd²⁺ to the surfaces of InP NCs almost completely eliminates electron trapping, whereas parallel chemistry with Zn2+ is somewhat less effective, and both show far less electron trapping than the native InP NC surfaces. This trend can be understood by recognizing that each surface In³⁺ requires three anions for complete charge compensation. When one or more of these charge-compensating anions is a surface carboxylate, a high density of surface ligands is required to avoid undercoordinated In³⁺, but such densities generate high steric pressures^{36,37} that favor partial ligand dissociation. We hypothesize that this steric pressure is partially relieved when some surface carboxylates are replaced with much smaller F⁻ anions, and also when surface In³⁺ cations are replaced with divalent Cd2+ or Zn2+ cations that only require two anionic ligands for charge compensation. Relief of steric pressure allows for better surface anion coordination and hence reduces the number of surface electron-trapping sites. The difference between Cd2+ and

 Zn^{2+} is also intriguing. Cd^{2+} completely eliminates surface electron trapping, but Zn^{2+} does not. We have previously shown that Cd^{2+} binds the InP NC surface more strongly than Zn^{2+} , 19,35 and this difference may account for the greater ability of Cd^{2+} to eliminate surface electron traps.

We note that our conclusion that undercoordinated In³⁺ serves as an electron trap contrasts recent computational results suggesting that L- and X-type vacancies at II–VI NC surfaces do *not* generate midgap trap states. In these calculations, only surface Z-type vacancies were found to generate midgap traps, in the form of anion-based hole traps. Because we observe an influence of our surface treatments on *electron* trapping, it appears that these conclusions drawn from calculations on II–VI NCs may not be transferrable to InP NCs. Indeed, other calculations⁶ performed specifically on InP NCs do suggest that indium "dangling bonds" introduce midgap electron traps, whereas phosphorus "dangling bonds" introduce midgap hole traps. Therefore, our experimental results are consistent with computational work on InP NCs.

Beyond their effect on InP NC PLQYs, the surface modifications described here also have interesting effects on other aspects of the NC PL. For example, the data show that the energy of the NC's first excitonic transition can be tuned in either direction by post-synthetic surface annealing with divalent cations, as detailed previously. 19,38 Less obvious is the observation that such submonolayer surface modification manifests itself in distinctive VTPL characteristics previously only observed with InP/ZnS^{32,39} and InP/ZnSe⁴⁰ core/shell NCs involving relatively thick passivating shells. Specifically, the InP/Cd and InP/F NCs show the unusual combination of decreasing short-time PL decay times but increasing short-time PL intensities with increasing temperature, and the data very closely resemble those of the thick-shelled InP NCs reported previously, where this temperature dependence was identified as a signature of thermal dark-bright exciton population equilibration. 40 At low temperatures, the fast PL decay is due to emission from a higher-energy bright state prior to relaxation into the lower-energy dark state, followed by slower emission from the forbidden dark state. 40 As the temperature is increased, the fast decay disappears, and the lifetime of the slow component decreases due to thermal population of the bright state. This behavior is not observed in our as-prepared InP NCs, most likely due to their fast nonradiative decay, and to our knowledge, such behavior has not been observed previously in any unshelled InP NCs. We note that other darkbright equilibria involving similar energy gaps and level ordering, for example, shallow reversible surface carrier trapping, could conceivably also generate a similar PL temperature dependence, but this interpretation of our data is viewed as less likely because the unusual temperature dependence emerges only upon elimination of electron trapping and therefore would have to involve shallow trapping of holes, but the trap-state PL energies observed for these NCs (e.g., Figures 2 and 3) indicate the presence of very deep hole traps. Instead, given the well-documented precedent of electronic dark-bright energy splittings stemming from carrier exchange interactions in core/shell InP NCs, 32,39,40 we prefer this interpretation of the data in Figures 3 and 4. It is also noteworthy that this transformation with surface modification is only apparent from VTPL data collected in the time domain. CW VTPL data for the InP, InP/F, and InP/Cd NCs all show decreasing intensities with increasing temperature, consistent with the presence of thermally activated nonradiative decay in

all three samples. Similar CW data have been reported elsewhere for unshelled InP NCs,²⁴ and in fact, most VTPL studies have focused on time-averaged data of shelled InP NC samples,^{13,24,25,29,32,39–42} but it is challenging to deduce any information about bright state population from such CW data. We conclude that the simple surface modifications described here can eliminate nonradiative recombination to a sufficient extent that these NCs behave photophysically similar to InP/ZnS and InP/ZnSe core/shell NCs with relatively thick passivating shells.

CONCLUSION

In summary, we have synthesized a homologous series of NCs originating from InP clusters and have used these NCs to study the effects of surface chemistry on charge-carrier trapping using a combination of TA, PL, and TRPL spectroscopies. Our data indicate that InP NC PLQYs can be increased substantially by simple surface chemical modifications that specifically eliminate surface electron traps. Cation binding strength (which dictates surface coverage), cation valency (which dictates obligate ligand density), and anion denticity and size (which together dictate ligand coverage and steric pressure) are all suggested to play prominent roles in the efficacy of electron trap suppression. The data further indicate that electron and hole trapping are roughly equally detrimental in the as-prepared InP NCs, such that even complete elimination of electron trapping by surface Cd²⁺ addition can only raise the NC PLQYs to ~50%, the remainder of the losses attributable to surface hole trapping. Such surface hole trapping can be partially suppressed by surface anion (rather than cation) modification. Notably, suppressing surface electron trapping unveils signatures of dark-bright exciton population dynamics that have never been observable in unshelled InP NCs before. Overall, the results presented here provide insights into chemical means of suppressing charge-carrier trapping at the surfaces of InP NCs, elevating the NC PLQYs, advancing our fundamental understanding of such traps and highlighting the use of targeted chemical modifications as tools for improving the photophysical properties of InP NCs relevant to their use as spectral conversion phosphor materials.

METHODS

General Considerations. All glassware was dried in a 160 °C oven overnight prior to use. All reactions, unless otherwise noted, were performed under an inert atmosphere of nitrogen using a glovebox or using standard Schlenk techniques. Myristic acid (≥99%), indium acetate (99.99%), anhydrous acetonitrile, anhydrous ethanol, zinc stearate, sulfur powder (99.5% sublimed), and selenium powder (99.99%) were purchased from Sigma-Aldrich Chemical Co. and used without further purification. Diethyl zinc (95%) and dimethyl cadmium (97%) were purchased from Strem Chemicals and stored in a nitrogen atmosphere glovebox. Toluene purchased from Sigma-Aldrich Chemical Co. was collected from a solvent still and stored over activated 3 Å molecular sieves in a glovebox. 1-Octadecene (1-ODE, 90%) and trioctylphosphine (TOP, 97%) were purchased from Sigma-Aldrich Chemical Co. and dried by being stirred overnight with CaH₂, distilled, and stored over activated 3 Å molecular sieves in a nitrogen atmosphere glovebox. Bio-Beads S-X1 for gel permeation chromatography were purchased from Bio-Rad Laboratories and dried under vacuum at elevated temperature before being stored in a glovebox. Cadmium oleate was prepared from dimethyl cadmium and oleic acid using a literature procedure.⁴³ Zinc myristate was prepared from diethyl zinc and myristic acid using a modified literature procedure. 19 TEM images were collected using a FEI Tecnai G2 F20 operating at 200 kV, and size distribution analysis was performed on 200–300 individual NCs per sample.

Synthesis of InP NCs. First, myristate-capped InP clusters were synthesized following a modified preparation and stored as a solid in a nitrogen atmosphere glovebox. 44,45 InP clusters (180 mg) were dissolved in 2 mL of 1-ODE and loaded into a septum-capped syringe. In a 50 mL 3-neck round-bottom (RB) flask, 34 mL of 1-ODE was heated to 300 °C under a nitrogen atmosphere on a Schlenk line. While stirring vigorously, the cluster solution was removed from the glovebox and rapidly injected into the flask. Upon injection, the solution turned dark red, and larger particle growth was monitored at 285 °C by UV-vis spectroscopy until the absorbance maximum no longer red-shifted (approximately 12 min). The solution flask was cooled down by placing it in an oil bath. The 1-ODE was removed through distillation under reduced pressure. The resulting NC paste was transferred into a glovebox for purification and redissolved in a minimal amount of toluene. To remove residual 1-ODE, a single precipitation cycle was performed with acetonitrile as the nonsolvent and centrifuge settings at 7000 rpm for 10 min. After removing the clear supernatant, the red pellet was dissolved in a minimal amount of toluene and purified by gel permeation chromatography, which has been commonly used in other nanoparticle purification approaches. 35,46 Briefly, 4 g of Bio-Beads were swollen overnight in 30 mL of anhydrous toluene and then packed into a column with a porous frit. The concentrated nanoparticle solution was injected into the column, and the colored fraction was collected. The resulting InP NC solution, free of excess ligand, was stored as a stock solution in toluene in the glovebox.

Preparation of InP/M NCs. InP/M NC samples were prepared following a modified procedure. ¹⁹ Using the InP NC stock solution, estimated to be 0.08 M In³⁺, 1 mL (0.08 mmol In³⁺) of solution was dried down and resuspended in 1-ODE. To produce InP/Zn, zinc myristate (64 mg, 0.12 mmol Zn²⁺) was suspended in 4 mL of 1-ODE and heated to 80 °C while stirring in a 15 mL 3-neck RB flask on the Schlenk line. The 1 mL solution of InP NCs was injected and heated to 200 °C. The reaction was halted after 2 h following no further changes in the absorbance or PL features. Particle purification was performed in the same fashion as the InP NCs. To produce InP/Cd, the same steps were followed with cadmium oleate (28 mg, 0.04 mmol) instead of zinc myristate.

Preparation of InP/ZnSeS NCs. InP NCs were coated with a ZnSeS shell following a modified literature procedure as described by Lee et al. 21 First, 1 M solutions of TOP-Se and TOP-S were prepared in the glovebox by dissolving selenium or sulfur powder in distilled TOP. Similar to the InP NC stock synthesis, a solution of InP NCs was prepared by injecting a solution of the myristate-capped InP clusters (20 mg, 0.045 mmol In³⁺, dissolved in 1 mL 1-ODE) into 5 mL of 1-ODE at 300 °C. Particle growth was monitored at 285 °C, and the reaction vessel was cooled down to 220 °C after no further changes were observed by UV-vis spectroscopy. For shell growth, zinc stearate (285 mg, 0.45 mmol) was injected as a suspension in 1-ODE (2 mL) and held at 220 °C for 15 min. Then, a solution containing TOP-S (45 uL, 0.045 mmol) and TOP-Se (405 uL, 0.405 mmol) was injected, and the temperature was raised to 300 °C and held for 60 min while monitoring the PL. After cooling down to room temperature, the solution was transferred into the glovebox and filtered with syringe filters (PTFE), and then the 1-ODE was removed by vacuum distillation. The resulting NC paste was purified with multiple precipitation cycles using toluene and ethanol as the solvent and nonsolvent, respectively.

Synthesis of InP NCs Treated with Fluoride-Containing Ionic Liquid. Under a nitrogen atmosphere, 10 mL of 1-octadecene was added, and the flask was heated to 290 °C. In a glovebox, 0.068 g (0.004 mmol) of InP clusters and 0.382 g (1.503 mmol) of 1-hexyl-3-methylimidazolium tetrafluoroborate (hmim BF4) were suspended in 2 mL of 1-octadecene. Note: The ionic liquid is immiscible in 1-octadecene at room temperature. The biphasic mixture was loaded into a plastic syringe and rapidly injected into the flask at 290 °C. The reaction vessel was stirred for 25 min after which the vessel was cooled to room temperature. The 1-octadecene was removed via

vacuum distillation, and the orange solid was dissolved in 5 mL of toluene and precipitated by addition of acetonitrile (approximately 10 mL). The supernatant was removed *via* centrifugation, and this process was repeated. The resulting solid was further purified *via* size-exclusion chromatography.³⁵

Spectroscopic Measurements. NCs were suspended in toluene and their absorption and CW PL spectra measured at room temperature. Absorption spectra were collected using a Cary 60 spectrophotometer (Varian). CW PL measurements were performed by exciting the colloidal NCs with a 405 nm laser diode and collecting the spectra using an OceanOptics 2000+ spectrometer. PLQY values were measured using an external quantum efficiency measurement system with a Hamamatsu Integrating Sphere (C9920-12) and a Hamamatsu high-sensitivity photonic multichannel analyzer (C10027-01). TA measurements were performed using an EOS unit from Ultrafast Systems at the University of Washington's Molecular Analysis Facility. The 800 nm output from a Coherent Libra amplified Ti:Sapphire laser (1 kHz repetition rate) was frequency-doubled using an OPA to excite the colloidal NCs in a 2 mm air-free cuvette with an average excitation power of \sim 5 μW measured through a 200 μ m pinhole. The NCs were stirred during the entirety of the experiment. The probe white light was generated using an external Q-switched Nd:YAG laser with an electronic delay. The collinear pump and probe beams overlapped at the sample. Room-temperature TRPL measurements were performed by exciting colloidal NCs with the frequency-doubled output of a Ti:Sapphire laser (400 nm, 150 fs pulse, power either 300 μ W or ~30 μ W, repetition rate either 1000 or 150 kHz). PL decay curves were recorded using a monochromator and streak camera (instrument response: ~25 ps). VT-TRPL measurements were performed on NC films fabricated by drop-casting colloidal NC solutions onto quartz discs, which were then placed in a closed-cycle cryostat. NC films were excited using the third harmonic of the 1064 nm fundamental output from a Nd:YAG laser with a 50 Hz repetition rate and an excitation energy of 1.3 µJ. The VT-TRPL dynamics and spectra were collected using a monochromator and streak camera (instrument response: ~ 20 ps).

ASSOCIATED CONTENT

S Supporting Information

The Supporting Information is available free of charge at https://pubs.acs.org/doi/10.1021/acsnano.9b07027.

Additional temperature-dependent TRPL dynamics, fitting parameters, and data analysis of PLQY and TA dynamics (PDF)

AUTHOR INFORMATION

Corresponding Authors

*E-mail: cossairt@uw.edu.

*E-mail: gamelin@chem.washington.edu.

ORCID 6

Kira E. Hughes: 0000-0001-6454-8700 Brandi M. Cossairt: 0000-0002-9891-3259 Daniel R. Gamelin: 0000-0003-2888-9916

Notes

The authors declare no competing financial interest.

ACKNOWLEDGMENTS

This research was supported by the U.S. National Science Foundation (NSF) through the UW Molecular Engineering Materials Center (MEM-C), a Materials Research Science and Engineering Center (DMR-1719797). Part of this work was conducted at the Molecular Analysis Facility, a National Nanotechnology Coordinated Infrastructure site at the University of Washington which is supported in part by the

National Science Foundation (grant NNCI-1542101), the University of Washington, the Molecular Engineering and Sciences Institute, and the Clean Energy Institute.

REFERENCES

- (1) Talapin, D. V.; Lee, J.-S.; Kovalenko, M. V.; Shevchenko, E. V. Prospects of Colloidal Nanocrystals for Electronic and Optoelectronic Applications. *Chem. Rev.* **2010**, *110*, 389–458.
- (2) Shirasaki, Y.; Supran, G. J.; Bawendi, M. G.; Bulović, V. Emergence of Colloidal Quantum-Dot Light-Emitting Technologies. *Nat. Photonics* **2013**, *7*, 13.
- (3) Tarantini, A.; Wegner, K. D.; Dussert, F.; Sarret, G.; Beal, D.; Mattera, L.; Lincheneau, C.; Proux, O.; Truffier-Boutry, D.; Moriscot, C.; Gallet, B.; Jouneau, P. H.; Reiss, P.; Carrière, M. Physicochemical Alterations and Toxicity of InP Alloyed Quantum Dots Aged in Environmental Conditions: A Safer by Design Evaluation. *Nano-Impact* 2019, 14, 100168.
- (4) Wegner, K. D.; Dussert, F.; Truffier-Boutry, D.; Benayad, A.; Beal, D.; Mattera, L.; Ling, W. L.; Carrière, M.; Reiss, P. Influence of the Core/Shell Structure of Indium Phosphide Based Quantum Dots on Their Photostability and Cytotoxicity. *Front. Chem.* **2019**, *7*, 466.
- (5) Tamang, S.; Lincheneau, C.; Hermans, Y.; Jeong, S.; Reiss, P. Chemistry of InP Nanocrystal Syntheses. *Chem. Mater.* **2016**, 28, 2491–2506.
- (6) Fu, H.; Zunger, A. InP Quantum Dots: Electronic Structure, Surface Effects, and the Redshifted Emission. *Phys. Rev. B: Condens. Matter Mater. Phys.* **1997**, *56*, 1496–1508.
- (7) Mićić, O. I.; Nozik, A. J.; Lifshitz, E.; Rajh, T.; Poluektov, O. G.; Thurnauer, M. C. Electron and Hole Adducts Formed in Illuminated InP Colloidal Quantum Dots Studied by Electron Paramagnetic Resonance. *J. Phys. Chem. B* **2002**, *106*, 4390–4395.
- (8) Kim, S. H.; Wolters, R. H.; Heath, J. R. Photophysics of Size-Selected InP Nanocrystals: Exciton Recombination Kinetics. *J. Chem. Phys.* **1996**, *105*, 7957–7963.
- (9) Langof, L.; Ehrenfreund, E.; Lifshitz, E.; Micic, O. I.; Nozik, A. J. Continuous-Wave and Time-Resolved Optically Detected Magnetic Resonance Studies of Nonetched/Etched InP Nanocrystals. *J. Phys. Chem. B* **2002**, *106*, 1606–1612.
- (10) Janke, E. M.; Williams, N. E.; She, C.; Zherebetskyy, D.; Hudson, M. H.; Wang, L.; Gosztola, D. J.; Schaller, R. D.; Lee, B.; Sun, C.; Engel, G. S.; Talapin, D. V. Origin of Broad Emission Spectra in InP Quantum Dots: Contributions from Structural and Electronic Disorder. J. Am. Chem. Soc. 2018, 140, 15791–15803.
- (11) Blackburn, J. L.; Ellingson, R. J.; Mićić, O. I.; Nozik, A. J. Electron Relaxation in Colloidal InP Quantum Dots with Photogenerated Excitons or Chemically Injected Electrons. *J. Phys. Chem. B* **2003**, *107*, 102–109.
- (12) Hahm, D.; Chang, J. H.; Jeong, B. G.; Park, P.; Kim, J.; Lee, S.; Choi, J.; Kim, W. D.; Rhee, S.; Lim, J.; Lee, D. C.; Lee, C.; Char, K.; Bae, W. K. Design Principle for Bright, Robust, and Color-Pure InP/ZnSe_xS_{1-x}/ZnS Heterostructures. *Chem. Mater.* **2019**, *31*, 3476–3484.
- (13) Kim, Y.; Ham, S.; Jang, H.; Min, J. H.; Chung, H.; Lee, J.; Kim, D.; Jang, E. Bright and Uniform Green Light Emitting InP/ZnSe/ZnS Quantum Dots for Wide Color Gamut Displays. *ACS Appl. Nano Mater.* **2019**, *2*, 1496–1504.
- (14) Kim, S.; Kim, T.; Kang, M.; Kwak, S. K.; Yoo, T. W.; Park, L. S.; Yang, I.; Hwang, S.; Lee, J. E.; Kim, S. K.; Kim, S.-W. Highly Luminescent InP/GaP/ZnS Nanocrystals and Their Application to White Light-Emitting Diodes. *J. Am. Chem. Soc.* **2012**, *134*, 3804–3809.
- (15) Mićić, O. I.; Cheong, H. M.; Fu, H.; Zunger, A.; Sprague, J. R.; Mascarenhas, A.; Nozik, A. J. Size-Dependent Spectroscopy of InP Quantum Dots. J. Phys. Chem. B 1997, 101, 4904—4912.
- (16) Talapin, D. V.; Gaponik, N.; Borchert, H.; Rogach, A. L.; Haase, M.; Weller, H. Etching of Colloidal InP Nanocrystals with Fluorides: Photochemical Nature of the Process Resulting in High Photoluminescence Efficiency. *J. Phys. Chem. B* **2002**, *106*, 12659–12663.

(17) Kim, T.-G.; Zherebetskyy, D.; Bekenstein, Y.; Oh, M. H.; Wang, L.-W.; Jang, E.; Alivisatos, A. P. Trap Passivation in Indium-Based Quantum Dots through Surface Fluorination: Mechanism and Applications. ACS Nano 2018, 12, 11529—11540.

- (18) Mićić, O. I.; Sprague, J.; Lu, Z.; Nozik, A. J. Highly Efficient Band-Edge Emission from InP Quantum Dots. *Appl. Phys. Lett.* **1996**, 68, 3150–3152.
- (19) Stein, J. L.; Mader, E. A.; Cossairt, B. M. Luminescent InP Quantum Dots with Tunable Emission by Post-Synthetic Modification with Lewis Acids. *J. Phys. Chem. Lett.* **2016**, *7*, 1315–1320.
- (20) Siramdas, R.; McLaurin, E. J. InP Nanocrystals with Color-Tunable Luminescence by Microwave-Assisted Ionic-Liquid Etching. *Chem. Mater.* **2017**, *29*, 2101–2109.
- (21) Lim, J.; Bae, W. K.; Lee, D.; Nam, M. K.; Jung, J.; Lee, C.; Char, K.; Lee, S. InP@ZnSeS, Core@Composition Gradient Shell Quantum Dots with Enhanced Stability. *Chem. Mater.* **2011**, 23, 4459–4463.
- (22) Jing, P.; Zheng, J.; Ikezawa, M.; Liu, X.; Lv, S.; Kong, X.; Zhao, J.; Masumoto, Y. Temperature-Dependent Photoluminescence of CdSe-Core CdS/CdZnS/ZnS-Multishell Quantum Dots. *J. Phys. Chem. C* 2009, *113*, 13545–13550.
- (23) Cho, E.; Kim, T.; Choi, S.-m.; Jang, H.; Min, K.; Jang, E. Optical Characteristics of the Surface Defects in InP Colloidal Quantum Dots for Highly Efficient Light-Emitting Applications. ACS Appl. Nano Mater. 2018, 1, 7106–7114.
- (24) Savchenko, S. S.; Vokhmintsev, A. S.; Weinstein, I. A. Effect of Temperature on the Spectral Properties of InP/ZnS Nanocrystals. *J. Phys.: Conf. Ser.* **2018**, *961*, No. 012003.
- (25) Narayanaswamy, A.; Feiner, L. F.; Meijerink, A.; van der Zaag, P. J. The Effect of Temperature and Dot Size on the Spectral Properties of Colloidal InP/ZnS Core—Shell Quantum Dots. ACS Nano 2009, 3, 2539–2546.
- (26) Ellingson, R. J.; Blackburn, J. L.; Yu, P.; Rumbles, G.; Mićić, O. I.; Nozik, A. J. Excitation Energy Dependent Efficiency of Charge Carrier Relaxation and Photoluminescence in Colloidal InP Quantum Dots. J. Phys. Chem. B 2002, 106, 7758–7765.
- (27) Thomas, A.; Sandeep, K.; Somasundaran, S. M.; Thomas, K. G. How Trap States Affect Charge Carrier Dynamics of CdSe and InP Quantum Dots: Visualization through Complexation with Viologen. *ACS Energy Lett.* **2018**, *3*, 2368–2375.
- (28) Hunsche, S.; Dekorsy, T.; Klimov, V.; Kurz, H. Ultrafast Dynamics of Carrier-Induced Absorption Changes in Highly-Excited CdSe Nanocrystals. *Appl. Phys. B: Lasers Opt.* **1996**, *62*, 3–10.
- (29) Rowland, C. E.; Liu, W.; Hannah, D. C.; Chan, M. K. Y.; Talapin, D. V.; Schaller, R. D. Thermal Stability of Colloidal InP Nanocrystals: Small Inorganic Ligands Boost High-Temperature Photoluminescence. *ACS Nano* **2014**, *8*, 977–985.
- (30) Klimov, V. I.; McBranch, D. W.; Leatherdale, C. A.; Bawendi, M. G. Electron and Hole Relaxation Pathways in Semiconductor Quantum Dots. *Phys. Rev. B: Condens. Matter Mater. Phys.* **1999**, *60*, 13740–13749.
- (31) Dennis, A. M.; Mangum, B. D.; Piryatinski, A.; Park, Y.-S.; Hannah, D. C.; Casson, J. L.; Williams, D. J.; Schaller, R. D.; Htoon, H.; Hollingsworth, J. A. Suppressed Blinking and Auger Recombination in Near-Infrared Type-II InP/CdS Nanocrystal Quantum Dots. *Nano Lett.* **2012**, *12*, 5545–5551.
- (32) Biadala, L.; Siebers, B.; Beyazit, Y.; Tessier, M. D.; Dupont, D.; Hens, Z.; Yakovlev, D. R.; Bayer, M. Band-Edge Exciton Fine Structure and Recombination Dynamics in InP/ZnS Colloidal Nanocrystals. ACS Nano 2016, 10, 3356–3364.
- (33) Chandrasekaran, V.; Tessier, M. D.; Dupont, D.; Geiregat, P.; Hens, Z.; Brainis, E. Nearly Blinking-Free, High-Purity Single-Photon Emission by Colloidal InP/ZnSe Quantum Dots. *Nano Lett.* **2017**, *17*, 6104–6109.
- (34) Stein, J. L.; Holden, W. M.; Venkatesh, A.; Mundy, M. E.; Rossini, A. J.; Seidler, G. T.; Cossairt, B. M. Probing Surface Defects of InP Quantum Dots Using Phosphorus $K\alpha$ and $K\beta$ X-Ray Emission Spectroscopy. *Chem. Mater.* **2018**, *30*, *6377*–*6388*.

(35) Roberge, A.; Stein, J. L.; Shen, Y.; Cossairt, B. M.; Greytak, A. B. Purification and *In Situ* Ligand Exchange of Metal-Carboxylate-Treated Fluorescent InP Quantum Dots *via* Gel Permeation Chromatography. *J. Phys. Chem. Lett.* **2017**, *8*, 4055–4060.

- (36) Gary, D. C.; Flowers, S. E.; Kaminsky, W.; Petrone, A.; Li, X.; Cossairt, B. M. Single-Crystal and Electronic Structure of a 1.3 nm Indium Phosphide Nanocluster. *J. Am. Chem. Soc.* **2016**, *138*, 1510–1513.
- (37) Cossairt, B. M. Shining Light on Indium Phosphide Quantum Dots: Understanding the Interplay among Precursor Conversion, Nucleation, and Growth. *Chem. Mater.* **2016**, *28*, 7181–7189.
- (38) Kirkwood, N.; Monchen, J. O. V.; Crisp, R. W.; Grimaldi, G.; Bergstein, H. A. C.; du Fossé, I.; van der Stam, W.; Infante, I.; Houtepen, A. J. Finding and Fixing Traps in II–VI and III–V Colloidal Quantum Dots: The Importance of Z-Type Ligand Passivation. J. Am. Chem. Soc. 2018, 140, 15712–15723.
- (39) Shirazi, R.; Kopylov, O.; Kovacs, A.; Kardynał, B. E. Temperature Dependent Recombination Dynamics in InP/ZnS Colloidal Nanocrystals. *Appl. Phys. Lett.* **2012**, *101*, No. 091910.
- (40) Brodu, A.; Ballottin, M. V.; Buhot, J.; van Harten, E. J.; Dupont, D.; La Porta, A.; Prins, P. T.; Tessier, M. D.; Versteegh, M. A. M.; Zwiller, V.; Bals, S.; Hens, Z.; Rabouw, F. T.; Christianen, P. C. M.; de Mello Donega, C.; Vanmaekelbergh, D. Exciton Fine Structure and Lattice Dynamics in InP/ZnSe Core/Shell Quantum Dots. ACS Photonics 2018, 5, 3353–3362.
- (41) Pham, T. T.; Chi Tran, T. K.; Nguyen, Q. L. Temperature-Dependent Photoluminescence Study of InP/ZnS Quantum Dots. *Adv. Nat. Sci.: Nanosci. Nanotechnol.* **2011**, *2*, No. 025001.
- (42) Narayanaswamy, A.; Feiner, L. F.; van der Zaag, P. J. Temperature Dependence of the Photoluminescence of InP/ZnS Quantum Dots. *J. Phys. Chem. C* **2008**, *112*, 6775–6780.
- (43) Stein, J. L.; Steimle, M. I.; Terban, M. W.; Petrone, A.; Billinge, S. J. L.; Li, X.; Cossairt, B. M. Cation Exchange Induced Transformation of InP Magic-Sized Clusters. *Chem. Mater.* **2017**, 29, 7984–7992.
- (44) Gary, D. C.; Terban, M. W.; Billinge, S. J. L.; Cossairt, B. M. Two-Step Nucleation and Growth of InP Quantum Dots *via* Magic-Sized Cluster Intermediates. *Chem. Mater.* **2015**, 27, 1432–1441.
- (45) Park, N.; Monahan, M.; Ritchhart, A.; Friedfeld, M. R.; Cossairt, B. M. Synthesis of In₃₇P₂₀(O₂CR)₅₁ Clusters and Their Conversion to InP Quantum Dots. *J. Visualized Exp.* **2019**, e59425.
- (46) Shen, Y.; Gee, M. Y.; Tan, R.; Pellechia, P. J.; Greytak, A. B. Purification of Quantum Dots by Gel Permeation Chromatography and the Effect of Excess Ligands on Shell Growth and Ligand Exchange. *Chem. Mater.* **2013**, *25*, 2838–2848.